The Importance of Explicitly Representing the Streambed in Watershed Models

Pin Shuai[1,2], Peishi Jiang[2], Ethan Coon[3], and Xingyuan Chen[2]

[1]Civil and Environmental Engineering, Utah Water Research Laboratory, Utah State University, Logan, Utah, USA
[2]Pacific Northwest National Laboratory, Richland, Washington, USA
[3]Climate Change Science Institute & Environmental Sciences Division, Oak Ridge National Laboratory, Oak Ridge, Tennessee, USA

Corresponding author: Pin Shuai, Pin.Shuai@usu.edu

Abstract

The streambed is the critical interface between the aquatic and terrestrial systems and hosts important biogeochemical hot spots within river corridors. Although the streambed characteristics are significantly different from those of its surrounding soil, the streambed itself has not been explicitly represented in watershed models. We developed an integrated hydrologic model that explicitly incorporated a streambed layer to examine the hydrological effects of streambed characteristics including hydraulic conductivity (K), layer thickness, and width on the exchange fluxes across the streambed as well as the streamflow at the watershed outlet. The numerical experiments were performed in the American River Watershed, a headwater, mountainous watershed within the Yakima River Basin in central Washington. Despite having a negligible effect on the watershed streamflow, an explicit representation of the streambed with distinctive properties dramatically changed the magnitude and variability of the exchange flux. In general, larger streambed K along with a thicker streambed layer induced larger exchange fluxes. The exchange flux was most sensitive to the streambed width or the mesh resolution of the streambed. A smaller streambed width (or a finer streambed resolution) increases exchange fluxes per unit area while reducing the overall exchange volumes across the entire streambed. The amount of baseflow decreased by 6% as the streambed width decreased from 250 m to 50 m. This finding is important because these hydrological changes may in turn affect the exchange of nutrients and contaminants between surface water and groundwater and the associated biogeochemical processes. Our work demonstrated the importance of representing streambed in fully distributed, process-based watershed models in better capturing the exchange flow dynamics in river corridors.

Keywords: streambed, surface water-groundwater interactions, hydrologic exchange flux, integrated watershed modeling

1 Introduction

The streambed is the critical interface between aquatic and terrestrial systems and hosts important hydrological and biogeochemical hot spots within watersheds. Streambed physical characteristics including hydraulic conductivity (K) play an important role in regulating the rate, timing, and location of surface water-groundwater exchange fluxes, which in turn impact the mobilization and transformation of nutrients and contaminants in river corridors (*Boano et al.*, 2014). Understanding the effects of streambed properties on watershed hydro-biogeochemical processes is crucial for watershed management and ecosystem health.

Past field and laboratory studies have found that streambed properties, especially streambed hydraulic conductivity (K), were considerably different from those of the underlying sediments. Streambeds tend to have reduced porosity and K due to fine sediment clogging and/or bioclogging (*Brunke*, 1999; *Shrivastava et al.*, 2020a). For example, *Levy et al.* (2011) measured the streambed K at different depths using seepage meters and slug tests and they found that the K in the top layer was an order of magnitude lower than the underlying sediments due to the deposition of fine sediments forming a heavily clogged top layer. On the contrary, streambeds influenced by sediment reworking (e.g., fish nesting) and scouring tend to have a larger K in the top layer (*Cardenas and Zlotnik*, 2003; *Song et al.*, 2010; *NOGARO et al.*, 2006). Even in the same river reach, streambed can exhibit strong heterogeneity in measured K that varies several orders of magnitude (*Datry et al.*, 2015). In addition to K, streambeds often vary in thickness and width, but the roles of those properties on exchange fluxes have received limited attention (*Ghysels et al.*, 2018).

Previous numerical studies using physically based models have primarily focused on the streambed- to channel-scale simulation of hydrological processes across various geomorphic settings (e.g., dunes, bars, and meanders) (*Boano et al.*, 2014). The heterogeneity of streambed sediments, bed thickness, bedform geometry, and channel curvature was found to control the rate and extent of hyporheic exchange (*Storey et al.*, 2003; *Salehin et al.*, 2004; *Cardenas et al.*, 2004; *Cardenas and Wilson*, 2007a,b; *Sawyer and Cardenas*, 2009). In meandering rivers, the river planimetry or sinuosity as well as channel bed slope have been shown to govern the pattern of intrameander hydrologic exchange flow paths (*Boano et al.*, 2006; *Cardenas*, 2009a,b; *Revelli et al.*, 2008; *Shuai et al.*, 2019; *Huang and Chui*, 2022). Most of these studies assumed idealized bed forms or meanders under steady-state flow conditions. Few modeling studies have simulated hydrologic exchange fluxes at river reach scale (100s of meter to 10s of km) or watershed scale that are driven by observed river morphology and natural flow conditions (*Zhou et al.*, 2018; *Shuai et al.*, 2019). Although these fine-scale studies provide detailed information about spatial and temporal patterns of streambed exchange fluxes, they do not scale to full watershed simulations.

Despite their distinctive properties, streambeds have not been explicitly represented in physically based, watershed models. Partly, this owes to the lack of observation data to parameterize streambeds in large watershed models. Watershed models have traditionally simplified the streambed representation and assumed homogeneous properties. There are two commonly used approaches for representing stream networks in physically based, watershed models. The first one is the channel routing approach, which is widely used by semi-distributed models (e.g., Soil and Water Assessment Tool (SWAT) and Precipitation-Runoff Modeling System (PRMS)). The stream network is predefined based on common hydrography datasets such as the NHDPlus (National Hydrography Dataset Plus, *Simley and Carswell Jr* (2009)). These models treat streams as simplified lines that connect via nodes. Each node stores information about streamflow upstream of the node. Within nodes, stream channels are conceptualized to be uniform with constant characteristics. This simplification improves computational efficiency at the watershed scale but ignores important processes including surface water-groundwater interactions and heterogeneous exchange flowpaths occurring at the terrestrial and aquatic interface.

The second approach to represent stream network is to form it naturally by following the terrains, which is used by most fully-distributed, integrated hydrologic models including ParFlow (*Kollet and Maxwell*, 2006), HydroGeoSphere (HGS) (*Aquanty*, 2015), and OpenGeoSys (*Kolditz et al.*, 2008). Instead of predefining stream networks, these models form stream networks from terrain-following grids. As a result, the location and width of the streambed are constrained by the topography and grid resolution of the model, which may deviate from the actual stream location and extent. For example, the ParFlow-CONUS model used a coarse grid resolution of 1 km on the land surface and results in overland flow routing of surface water across 1-km grid cells (*Maxwell et al.*, 2015). The coarse meshes lead to zigzagging river channels, while the averaging of channel topography and slopes across the mesh element results in reduced stream water depth and velocity. Typically, these integrated hydrologic models also assume that the streambed meshes share the same physical properties as the soil or geologic layer underneath them.

To accurately represent the streambed in a watershed-scale model, a fine grid resolution near stream channels, both horizontally and vertically, is desired. The grid resolution is highly important for the spatial representation of channel topography, which affects fine-scale hyporheic exchange across bedforms (e.g., bars, pools, and riffles) (*Boano et al.*, 2007) and stream-riparian zone interactions (e.g., overbank flooding) (*Dey et al.*, 2022; *Marks and Bates*, 2000). A recent study found that 85% of global rivers have an average width of 150 m (*Feng et al.*, 2022). For headwater streams, the width would be much smaller. Using a coarse resolution mesh at the watershed scale would likely obliterate small creeks and low-order streams (*Käser et al.*, 2014). However, refining meshes uniformly across the watershed (i.e., structured meshes) would exponentially increase the total number of grid cells, and thus the associated computational cost. To balance the computational cost and model resolution, unstructured meshes which use a finer grid near the domain of interest and a coarser grid elsewhere have been adopted in integrated hydrologic models (e.g., HGS).

Previous studies have neither explicitly represented streambed nor examined the hydrologic exchange flux patterns in watershed models. The objective of this study is to investigate the effects of streambed properties on watershed hydrological processes such as the exchange flux between surface water and groundwater. We achieve this by explicitly representing the streambed in Advanced Terrestrial Simulator (ATS), an integrated hydrologic model that couples surface-subsurface flows with land surface processes, using unstructured meshes. The variable meshes in both horizontal and vertical directions allow the fine-scale streambed morphology to be fully resolved while saving computational costs. We test the sensitivity of streambed K, layer thickness, and streambed width (or horizontal grid resolution) on the hydrologic exchange flows across streambeds as well as watershed streamflow in a mountainous, headwater watershed. Our study has important implications for simulating groundwater/stream interactions and the associated biogeochemical processes at the watershed scale.

2 Material and Methods

2.1 Study site

The American River Watershed is a headwater watershed located within the Yakima River Basin in Central Washington (Figure 1). The watershed receives an annual average precipitation of ~1740 mm. As a snow-dominated watershed, snowfall contributes nearly half of the precipitation, with an annual average of ~850 mm, and primarily occurs from December through April. The watershed is classified as a Mediterranean-influenced warm-summer humid continental climate (i.e., Dsb) on the Koppen classification system. It is a HUC10 watershed that encompasses 205 km^2 area with evergreen (83%) and shrub land (11%) as the two dominant land cover types. There is one USGS gage (12488500) located at the watershed outlet with gage height and discharge measurements.

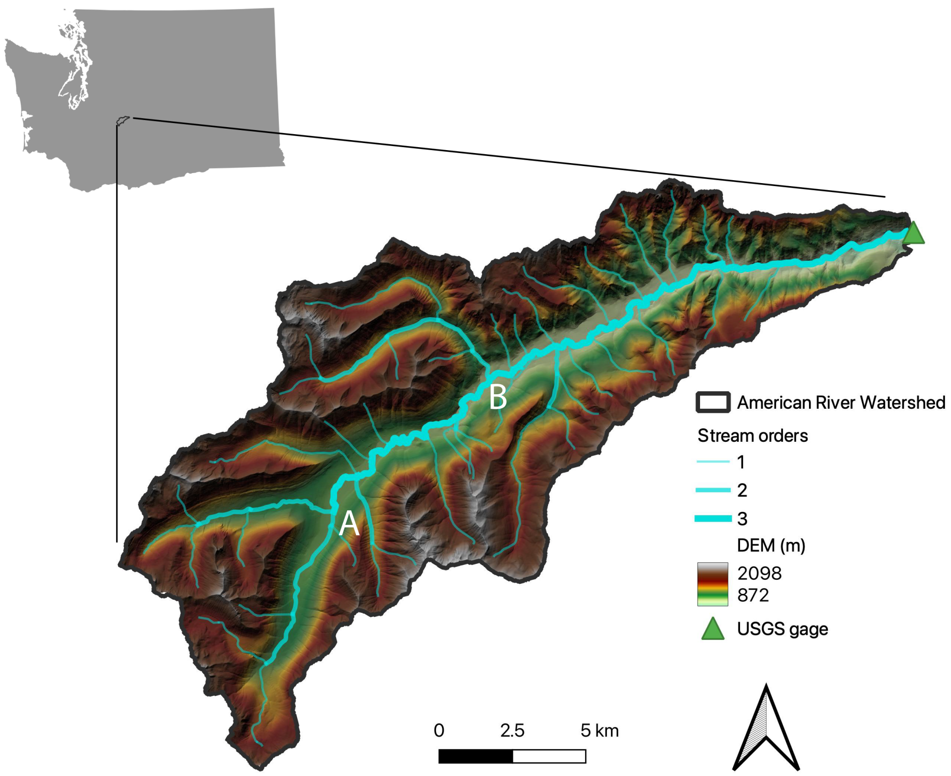

Figure 1. Study site showing the location of the American River Watershed within Washington State, DEM, and stream network within the watershed. USGS gage is indicated in a green triangle.

2.2 ATS model setup and initialization

The Advanced Terrestrial Simulator (ATS) is an integrated surface-subsurface, distributed hydrologic model that computes the diffusion wave approximation of the 2-D St-Venant equations for overland flow and the 3-D Richards equation for groundwater flow (*Coon et al.*, 2019, 2020). Energy balance equations are used to simulate land surface processes such as ET and snowmelt. The code's high performance enables it to be parallelized on supercomputers, allowing it to run on hundreds to thousands of processors simultaneously.

The Watershed Workflow Python package (v1.2) was used to create the baseline model (*Coon and Shuai*, 2022). This package combines multiple data streams, identifies the watershed area, and produces a variable resolution mesh with a more refined resolution near the stream network. The mesh is triangular in shape and was created using the Digital Elevation Model (DEM) from the National Elevation Dataset (NED) with a 30 m resolution. The mesh's horizontal resolution varied from 250 m near the stream network to 320 m further away.

For the subsurface, the domain was divided into 16 terrain following layers, with a total thickness of 24 m. The top 2 m of the domain is made up of soil layers, and the vertical resolution of the mesh increased from 0.25 m at the surface to 2 m at the bottom. The thickness of the first five layers is 0.25, 0.25, 0.5, 1.0, and 2.0 m, respectively, while the remaining layers are 2m thick. The model consists of 125,664 cells, and the depth-to-bedrock (DTB) ranges from 6.5 m to 24.1 m as determined from SoilGrids (*Shangguan et al.*, 2017). The geologic layers are sandwiched between the soil and bedrock layers.

The SSURGO soils database was used to identify and map 52 distinct soil types within the soil layer. Similarly, 11 different types of raw geologic materials were identified and mapped within the geologic layer using data from the GLHYMPS 2.0 dataset (*Huscroft et al.*, 2018). The permeability and porosity values were obtained from the SSURGO database. Soil properties from SSURGO was then used in conjunction with Rosseta v3, a pedotransfer function that relates the percentages of sand, silt, and clay to van Genutchen parameters, as described by (*Zhang and Schaap*, 2017). For the geology types, the permeability and porosity values were retrieved from the GLHYMPS database. A confining layer was assumed to exist due to the negligible permeability ($1\times10^{-17}\ m^2$) of the bedrock.

The model was first initiated for 1000 years using the annual mean precipitation ($\sim 1690\ mm/yr$) as the spin-up. This resulted in steady state model outputs at the final timestep, which was then used as the initial condition for a 10-year transient simulation. The transient simulation was driven by smoothed meteorological forcing data obtained from the DayMet dataset (*Thornton et al.*, 2021). The model state at the end of the 10-year transient run was used as the initial condition for the transient run shown in the Results section, which occurred from October 1, 2013, to October 1, 2016. The DayMet forcing data is a gridded dataset with a resolution of 1 km and covers the entire North American region. Precipitation, air temperature, incoming shortwave radiation, and vapor pressure data were mapped onto the meshes and prescribed throughout the simulation.

2.3 Model calibration

The model was calibrated using a newly developed knowledge-informed deep learning approach (*Jiang et al.*, 2022). The approach leverages mutual information (MI)-based sensitivity analysis to guide the selection of the sensitive model responses (e.g., streamflow) which is used to estimate each parameter based on a neural network. The previous study successfully employed this approach to calibrate ATS in another snow-dominated watershed using a few hundred realizations. Due to a large number of uncertain parameters, both soil and geology types were simplified using k-mean clustering to reduce the number of parameters for calibration. The spatial distribution of the clustered soil and geological layers is shown in Figure 2. A MI-based preliminary sensitivity analysis was first performed to narrow down the parameters to be calibrated using 50 ensemble runs. This leads to a total of 14 parameters to be calibrated, including five soil permeability (i.e., s1, s3, s4, s5, and s6), three geologic layer permeability (i.e., g1, g2, and g4), three evapotranspiration (ET) parameters (i.e., Priestly_Taylor_alpha-canopy_transpiration, Priestly_Taylor_alpha-snow_evaporation, and Priestly_Taylor_alpha-ground_evaporation), two snowmelt parameters (i.e., snowmelt_rate and air-snow_temperature_difference), and one Manning's coefficient (i.e., manning_n). Then, 323 ensemble runs were generated by varying the down-selected 14 parameters to perform a full sensitivity analysis and model calibration. Each run consisted of three years of simulation (i.e., October 2013 - October

2016) with the last two years being used as the calibration period. For each parameter, an inverse mapping was constructed based on a fully-connected neural network to estimate the parameter from the corresponding sensitive streamflow observations. Ensemble runs were used to train and tune the structure of the neural network. Observations were used to estimate the parameters through the trained neural network.

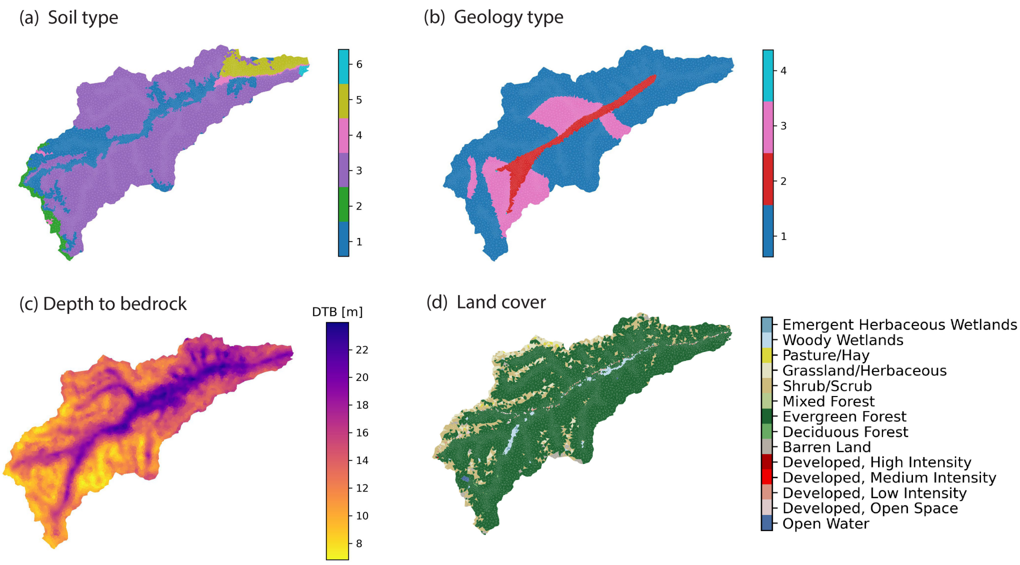

Figure 2. Watershed inputs include soil type, geology type, depth to bedrock and land cover type as generated using the Watershed Workflow v1.2. The soil and geology types have been clustered using k-mean clustering.

2.4 Streambed characteristics

Streambed geometry such as width and depth was determined based on the discretization of the meshes (Figure 3). To examine the effects of streambed width, we applied different refinements near the stream network to make the finest mesh resolution close to the targeted streambed width (e.g., 50 m, 150 m and 250 m). For different mesh refinements, only the meshes near the streams were refined while keeping the meshes near the boundary at a coarser resolution ($\sim 300\ m$). The streambed was then determined by the meshes that overlap with the river network. The streambed depth was determined based on vertical discretization. For example, a streambed with a width of 250 m and a thickness of 0.5 m indicates that the streambed consists of meshes with an average horizontal resolution of 250 m located within the top 0.5 m. The entire streambed was assigned the same property.

To investigate the effects of streambed properties, we systematically varied the streambed K from 0.1 to 10 m/d and thickness from 0.25 to 1.0 m based on the reported literature values (Table 1) (*Calver*, 2001; *Cardenas and Zlotnik*, 2003; *Genereux et al.*, 2008). For example, the streambed K was found to range from 0.001 to 100 m/d based on 41 different field and numerical studies (*Calver*, 2001). Our baseline model assumed zero thickness of the riverbed and the river region shared the same K values with the underlying sediments.

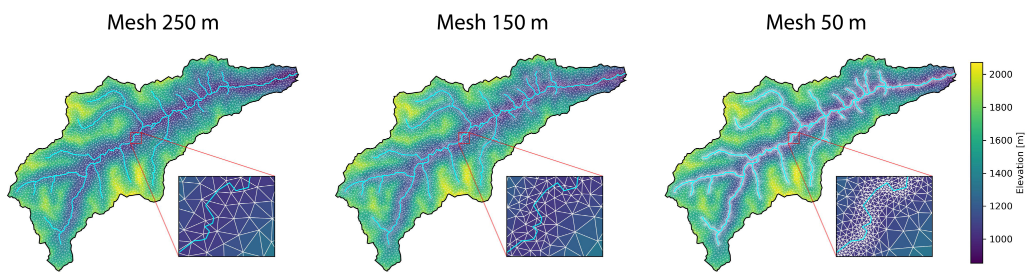

Figure 3. Watershed meshes in different streambed resolutions. The zoomed-into insert shows the finest mesh near the stream network.

Table 1. Model cases with various sets of streambed K, thickness, and width

Case	Streambed K [m/d]	Streambed thickness [m]	Streambed width [m]
base	same as soil K	0.0	250
1	1.0	0.5	250
2	0.1	0.5	250
3	0.1	0.5	250
4	1.0	0.25	250
5	1.0	1.0	250
6	1.0	0.5	50
7	1.0	0.5	150

3 Results

The calibrated model showed good performance in simulated versus observed streamflow (mKGE=0.62) (Figure 4). The following results focused on hydrologic exchange fluxes across the streambed as well as the streamflow at the watershed outlet.

3.1 Exchange fluxes across the streambed–baseline case

The exchange flux showed strong spatial and temporal heterogeneity across streambeds in response to precipitation events. Temporally, the river was predominantly gaining (i.e., flow from the groundwater into the river) all year round as indicated by the positive mean exchange fluxes (Figure 5(A)). The river was relatively more gaining during the snowmelt and rainfall period in the winter and spring compared to that during the dry period in the summer. For example, Figure 5(B) showed the spatial distribution of the exchange flux across the streambed on April 1st, 2015, and October 1st, 2015, which corresponded to the peak of the wet (April) and dry (October) season of that year. Those two selected snapshots showed large differences in the magnitude as well as the directions of the exchange fluxes. In general, the river was less gaining and losing in the dry season compared to that in the wet season.

Spatially along the main stem (i.e., 3rd order stream), the river showed hot spots of exchange fluxes at several locations, especially during large precipitation events (Figure 5A). The heat map of exchange fluxes across the main stem was plotted from the farthest upstream location (i.e., 22 km) to the outlet (i.e., 0 km). These hot spots of exchange fluxes corresponded to the locations of confluence and geomorphic features such as meanders. For example, at the start of the main stem (22 km from the outlet, Location A in Figure 1), the main stem of the stream was strongly gaining as it was

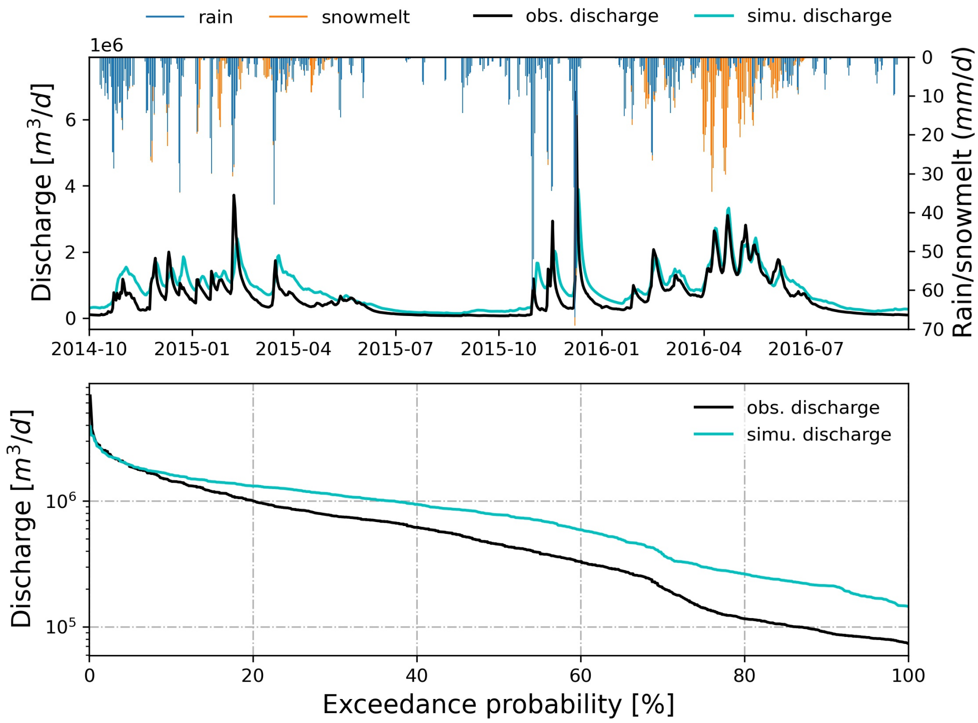

Figure 4. Simulated streamflow shows good performance (KGE=0.62) against observed streamflow using the calibrated baseline model.

joined by two subcatchments in the headwaters. Similarly, the river was gaining during snowmelt and large precipitation events at a distance of 15 km from the outlet (location B in Figure 1) as the main stem was joined by a large tributary on the left side of the river. The exchange flux also showed large variation by stream orders (Figure S1). The second-order stream had the largest variability and median value, whereas the first- and third-order streams showed less variability. Though all streams were primarily gaining, a significant portion of the second-order stream was losing.

3.2 Effects of streambed hydraulic conductivity and thickness

Larger streambed hydraulic conductivity induced larger exchange fluxes across the streambed, assuming the streambed thickness and width were the same (Figure 6). The differences were larger in the wet season compared to those in the dry season. By changing K from 0.1 to 10 m/d, the mean exchange flux increased from 16.6 mm/d to 19.3 mm/d, though the differences in streamflow at the watershed outlet were insignificant (Figure S2). In comparison, the exchange flux under the baseline model was almost identical to that under K=10 m/d.

Larger streambed thickness induced smaller exchange fluxes across the streambed, assuming the streambed K and width remained the same (Figure 6). This also assumed streambed K (i.e., 1 m/d) was smaller than the K of the surrounding soil/geology sediments. Similarly, the largest difference in exchange flux occurred in the wet period, whereas the smallest difference occurred in the dry period. By changing thickness from 0.25 m to 1.0 m, the mean exchange flux decreased from 17.9 mm/d to 15.6 mm/d, though the discharge at the watershed outlet remained unchanged (Figure S3). In comparison, the exchange flux from the baseline model was equal to or larger than that under a thickness of 0.25 m since the streambed layer did not exist in the baseline model.

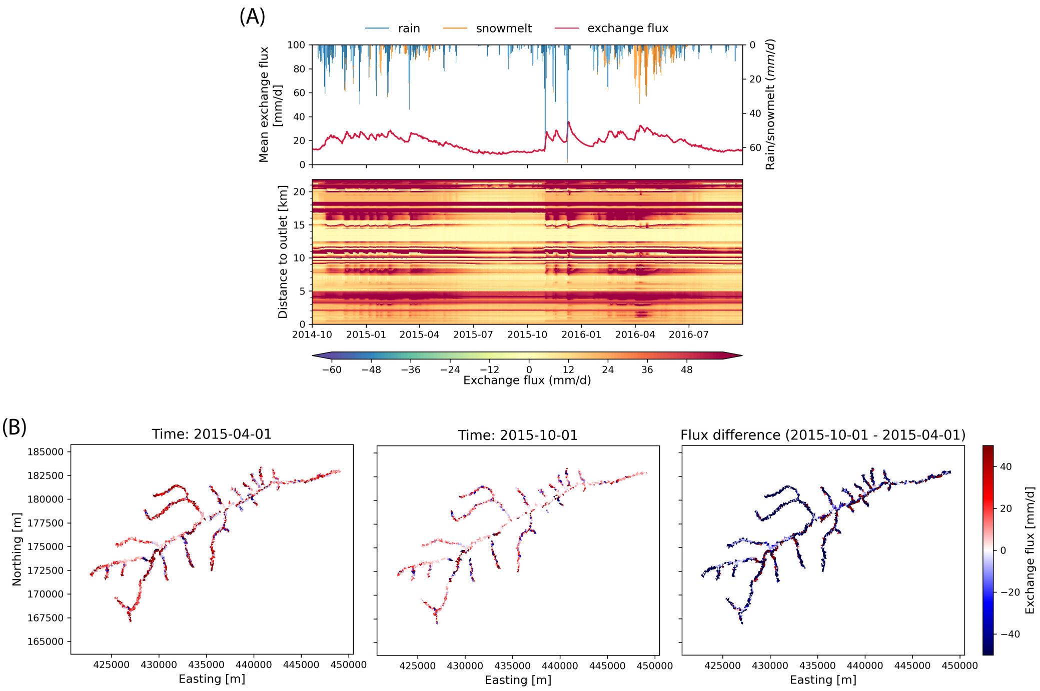

Figure 5. Sptial and temporal variability of exchange fluxes across streambeds. **(A)** Exchange flux heat map across the main stem (i.e., third-order) stream shows strong spatial and temporal variability. **(B)** Snapshots show exchange fluxes across the streambed during wet (April 1, 2015) versus dry (October 1, 2015) period as well as the flux differences between those two snapshots.

3.3 Effects of streambed width (resolution)

A smaller streambed width (or finer streambed resolution) induced larger exchange fluxes per unit area, but with an overall smaller exchange volume across the whole watershed (Figure 7). By refining the streambed width from 250 m to 50 m, the mean exchange flux increased from 17.7 mm/d to 45.8 mm/d, which was a 150% increase. On the contrary, the total exchange flux across the entire streambed decreased from 3.58e5 m^3/d to 1.79e5 m^3/d as the streambed resolution increased from 250 m to 50 m. The cumulative exchange volume during the two-year period showed a 50 % decrease. In comparison, the exchange flux from the baseline model showed similar exchange flux magnitude and patterns with those from the 250-m width model due to the same streambed resolution being used.

Within each stream order, smaller streambed width showed larger exchange fluxes in both magnitude and variability (Figure 8). Across stream orders, the third-order stream showed the largest median exchange flux, whereas the second-order stream showed the largest variability. However, as the stream width decreased (or resolution increased), the median exchange flux in the second-order stream became significantly ($p < 0.05$ using a Mann-Whiteney U test) smaller than those in the other stream orders. The results highlighted the importance of using a finer streambed resolution to capture the exchange flux patterns across and within stream orders.

The accumulative baseflow was lower under a smaller streambed width (or a finer resolution) (Figure 9), though the watershed discharge showed a marginal difference (Figure S4). By refining the streambed width from 250 m to 50 m, the temporal baseflow flux decreased especially in the

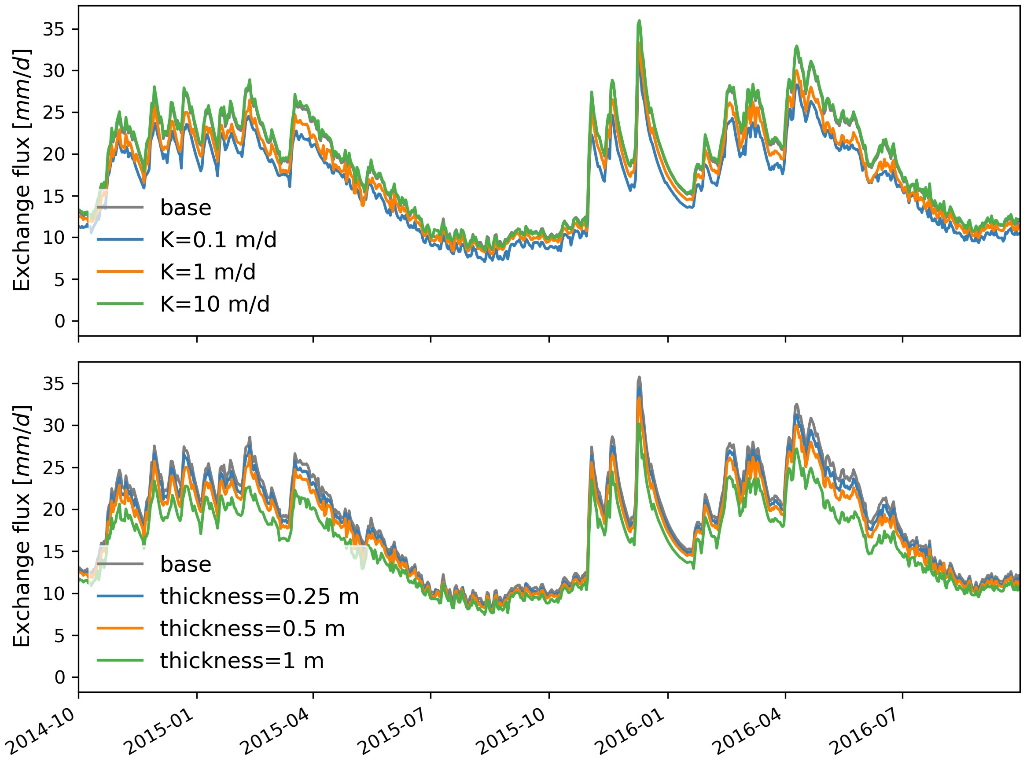

Figure 6. Larger streambed K induces larger exchange fluxes. Larger streambed thickness induces smaller exchange fluxes. In reference, the baseline model has K ≈ 10 m/d and thickness = 0 m.

wet period. The accumulative baseflow decreased from 1.54 m to 1.45 m per watershed area (a 6% decrease). The percentage of baseflow relative to the watershed discharge decreased from 51% to 48%.

4 Discussion

4.1 Is an explicit representation of streambed important?

Without an explicit representation of the streambed, the watershed model using the default permeability of the soil on top tends to overestimate the exchange flux. Compared to the baseline model, an explicit representation of a streambed with different K and thickness showed a significant difference in both exchange flux magnitude and variability (Figure 6). In general, streambeds with a larger K combined with a thicker layer promoted the hydrologic exchange fluxes between the river and aquifer. However, the shallower streambed sediment usually has a lower K than the deeper sediments due to abiotic (fine sediments) and biotic (microorganisms) clogging (*Datry et al.*, 2015; *Min et al.*, 2013; *Shrivastava et al.*, 2020b). For example, *Min et al.* (2013) showed that the K measured from a clogged streambed was 3 to 4 orders of magnitude lower than that measured from an unclogged streambed. Without a representation of the less permeable streambed layer, the exchange fluxes would be overestimated as shown in Figure 6.

To represent the streambed layer, streambed properties including K and thickness are required as model inputs, however, they are rarely available and are difficult to measure especially across the entire watershed (*Korus et al.*, 2020; *Abimbola et al.*, 2020). Traditionally, streambed K is measured using slug tests or inferred from the grain size distribution of the sediment, which is labor-intensive

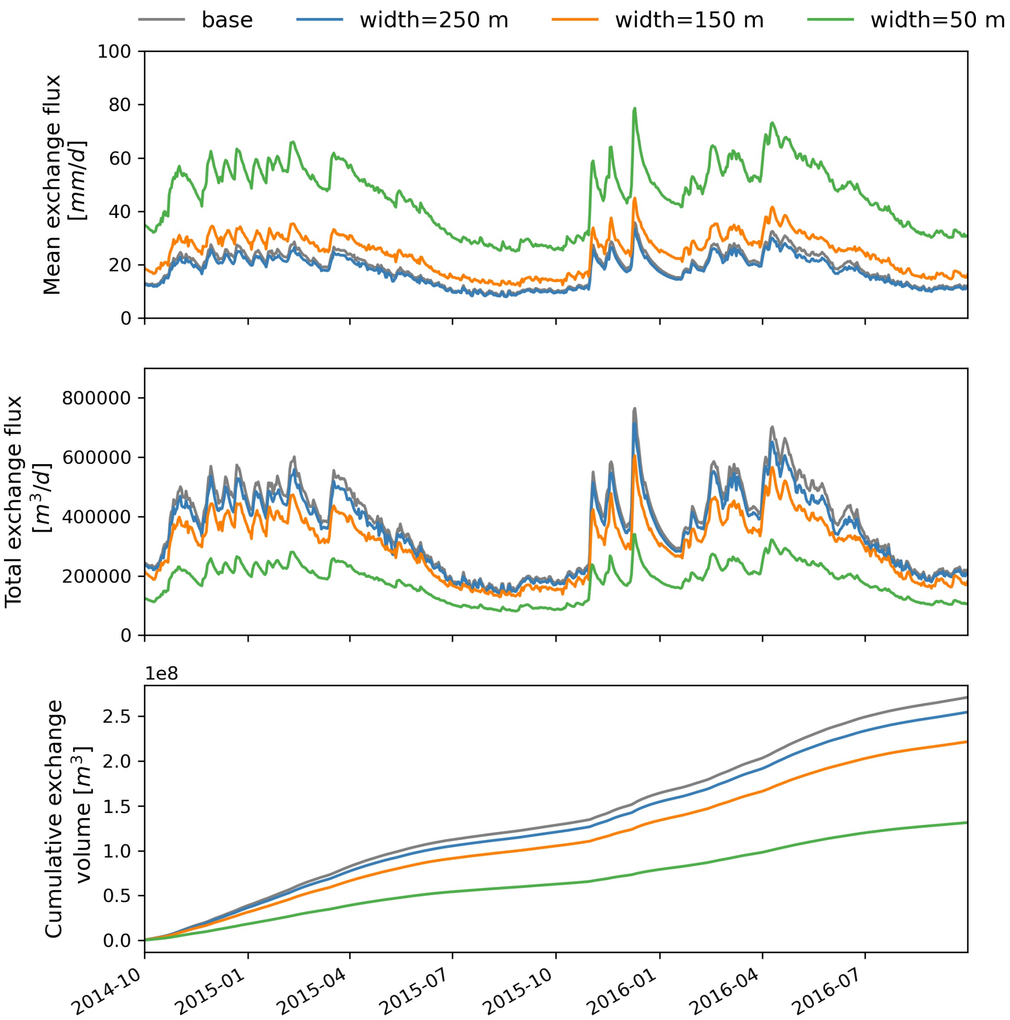

Figure 7. Larger streambed width (resolution) induces smaller exchange fluxes per unit area but overall larger exchange flux volume. In reference, the baseline model has a streambed width of 250 m.

and cannot be easily scaled up to the entire watershed. Recently, *Abimbola et al.* (2020) developed new pedo-transfer functions using the Multi-Stemmed Nested Funnel approach to predict the vertical streambed K variability based on watershed characteristics including drainage area and percent organic matter, which are readily available in the National Resources Conservation Service (NRCS) Soil Survey Geographic (SSURGO) soils database. This provides a cost-effective way to estimate the spatial distribution of streambed K across different stream orders.

4.2 Is a high-resolution streambed needed for watershed simulations?

Mesh resolution has a marginal impact on the watershed outlet discharge. This is because the percentage of streambed area in our study site is less than 15% of the entire watershed area, which had little impact on the overland flow processes. Additionally, the majority of the watershed mesh resolution remained constant due to the refinement only occurring near the stream network. As a result, most of the topography and land cover remained the same, especially in the high elevation where snow accumulated. The watershed discharge would become more sensitive to the

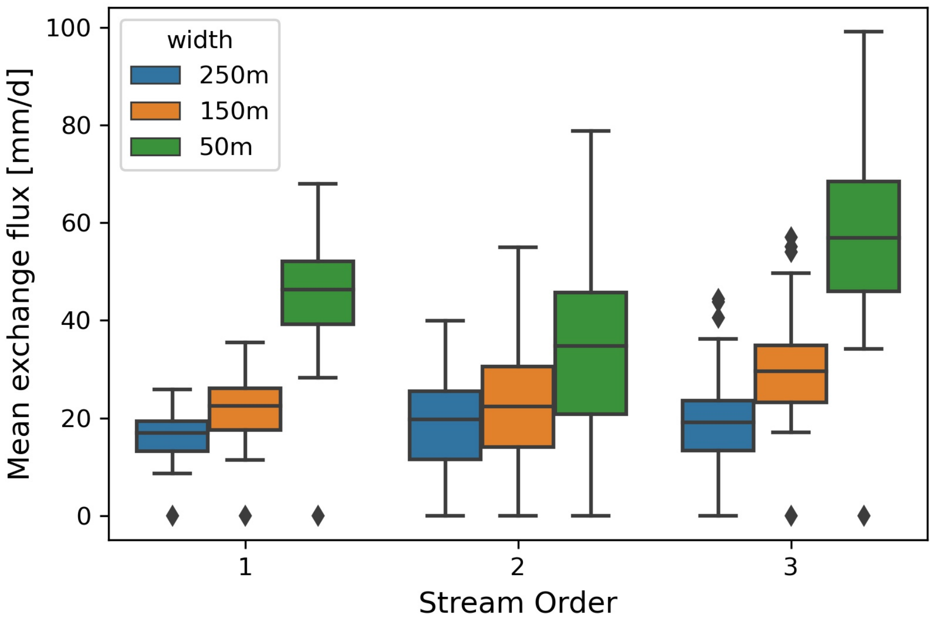

Figure 8. A boxplot showing the variability of exchange flux across different stream orders under different streambed widths. Within each stream order, smaller streambed width showed larger exchange fluxes in both magnitude and variability. Across stream orders, the third-order stream showed the largest median exchange flux, whereas the second-order stream showed the largest variability.

mesh resolution if it is uniformly changed across the landscape (*Sulis et al.*, 2011; *Foster et al.*, 2020). *Foster et al.* (2020) found that uniformly coarsening the mesh from 100 m to 1 km resulted in a 4% reduction in predicted streamflow under climate change using ParFlow. The decrease in the streamflow as a result of mesh coarsening was mainly due to the decrease in local terrain slope and plan curvature variation, which limited the amount of water transmitted laterally and downslope (*Sulis et al.*, 2011). On the contrary, streambeds with a coarse mesh resolution slightly overestimated the watershed base flow (Figure 9). The accumulated base flow increased by 6% as the streambed resolution decreased from 50 m to 250 m. The increase in base flow was the result of a larger streambed area represented in the coarser streambed resolution model, which facilitated groundwater exfiltration out of the streambed.

Models using coarse streambed resolutions underestimate the magnitude and variability of exchange fluxes but overestimate the total exchange volume (Figure 7). They also undermine the relative difference in the exchange flux variability among different stream orders (Figure 8). This is mainly due to the fact that a finer mesh resolution model better preserves the topographic features such as meanders, pools, and riffles, which have been demonstrated to be the hot spots of exchange fluxes (*Shuai et al.*, 2019; *Cardenas*, 2008; *Tonina and Buffington*, 2007). In a previous study, *Brookfield et al.* (2017) showed that increasing mesh resolution along the streambed allowed for the topography-driven exchange flux variability to be accounted for using HydroGeoSphere.

The variability and magnitude of exchange fluxes across the streambed are the main drivers for hot spots and hot moments of biogeochemical reactions in river corridors (*Dwivedi et al.*, 2018; *Zarnetske et al.*, 2011; *Shuai et al.*, 2017). Without a high-resolution model, the biogeochemical reactions could be greatly underestimated. For example, our results showed that the mean exchange flux per unit area was greatly increased along with its variability under a 50 m resolution compared

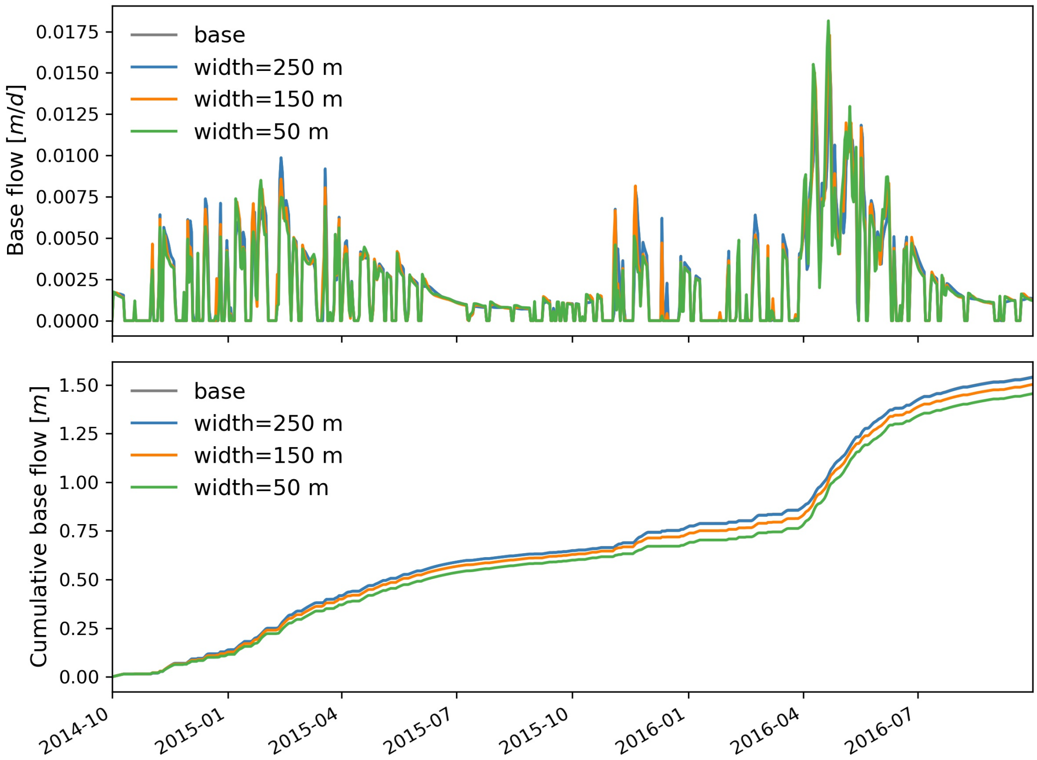

Figure 9. The cumulative base flow decreased slightly as the streambed width decreased from 250 m to 50 m while the streambed thickness (0.5 m) and K (1 m/d) remain the same. The base flow under the baseline model overlaps with that of the 250 m resolution model.

to that under a 250 m resolution (Figure 7 and 8). The larger exchange fluxes in the 50 m resolution model may promote the exchange of nutrients between surface water and groundwater and impact the associated biogeochemical processes in the watershed.

In summary, a high-resolution streambed is preferred if exchange fluxes and biogeochemical processes are of interest. Distributed watershed models should refine the meshes near the streambeds to accurately capture the exchanges between surface water and groundwater. However, the streambed mesh resolution plays an insignificant role in watershed streamflow generation.

4.3 Limitations and future work

Using high-resolution streambeds in integrated hydrologic models increases the computational cost. Even though we can save computational cost by taking the advantage of unstructured meshing capability, the total number of grid cells still significantly increases as the streambed is further refined. For example, by refining meshes from 250 m to 50 m in ATS, the total number of grid cells increased from 125,664 to 621,968, a five-fold increase. In our study, it took $\sim$ 17 hrs for the 50-m model to finish three years of simulation using 256 cores compared to $\sim$ 4 hrs for the 250-m model to finish the same number of years using 64 cores. In headwater streams, the actual streambed width may be even smaller (e.g., 10 to 20 m), and thus requires further mesh refinement near the stream network. If 10 m mesh resolution were used for our watershed, the total number of meshes would be over 3 million. The computational cost would be unmanageable despite the increase in computational power offered by high-performance computing systems.

High-resolution models often require high-resolution datasets and extensive parameterization. Recent remote sensing product enables the DEM to be mapped at 1 m or less resolution. However, the river bathymetry data is not widely available in most watersheds, which is critical for representing fine-scale river morphology including bars, pools, and riffles. The bathymetry data becomes more important in higher-order streams due to larger variability in river bathymetry. Fortunately, estimating river bathymetry in rivers wider than 50 m will become possible thanks to the newly launched Surface Water and Ocean Topography (SWOT, https://swot.jpl.nasa.gov, last accessed on January 4, 2023) satellite. SWOT will provide water surface elevation, width, and slope that could be used as input to inverse models to retrieve river bathymetry and roughness coefficients (*Yoon et al.*, 2012).

Assuming homogeneity of K across the streambeds in watershed models often leads to the under- or over-prediction of exchange fluxes across the streambed (*Abimbola et al.*, 2020). Streambed K is highly heterogeneous with K varying several orders of magnitude even in the same stream order. For example, higher K usually occurred in upwelling versus downwelling areas (*Datry et al.*, 2015). However, there is a lack of data to quantify the heterogeneous distribution of streambed K, and it is not practical to measure it everywhere.

In the future, we plan to quantify the effects of exchange fluxes on watershed biogeochemical cycling by incorporating biogeochemical reactions into the watershed hydrologic models. This can be accomplished by coupling ATS with PFLOTRAN via the Alquimia interface (*Andre et al.*, 2013), which has been demonstrated in a recent publication (*Molins et al.*, 2022).

5 Conclusions

We investigated the effects of streambed properties including hydraulic conductivity, layer thickness, and width (resolution) on watershed hydrological processes by explicitly representing streambed in an integrated watershed model. To the best of our knowledge, this is the first of its kind study to illustrate the role of streambed representation and its properties on exchange fluxes between surface water and groundwater at the watershed scale. Our results showed that the exchange flux was spatially and temporally heterogeneous across different stream orders in response to precipitation events. Watershed models without an explicit representation of the streambed tend to overestimate the exchange flux, though its impact on watershed streamflow is negligible. Generally, larger streambed hydraulic conductivity along with a thicker streambed layer induced larger exchange fluxes. The exchange fluxes were most sensitive to the streambed width or the mesh resolution of the streambed. A smaller streambed width (or finer streambed resolution) induced larger exchange fluxes per unit area, but smaller exchange volume across the entire streambed. As a result, The amount of baseflow decreased by 6% as the streambed width decreased from 250 m to 50 m. Within each stream order, a model with smaller streambed width showed a larger exchange flux in both magnitude and variability, which may promote the exchange of nutrients and contaminants between surface water and groundwater, resulting in hot spots and hot moments of biogeochemical reactions. Our study calls for the high-resolution representation of streambeds in watershed models when hydrologic exchange fluxes and biogeochemical processes are of particular interest. Future studies should focus on characterizing the heterogeneity of streambeds through the advanced field and statistical methods to parameterize watershed models.

Acknowledgments
This research was supported by the U.S. Department of Energy (DOE), Office of Biological and Environmental Research (BER), as part of BER's Subsurface Biogeochemical Research Program (SBR). This contribution originates from the SBR Scientific Focus Area (SFA) at the Pacific Northwest National Laboratory (PNNL). PNNL is operated for the DOE by Battelle Memorial Institute under contract DE-AC05-76RL01830. This research used resources of the National Energy Research Scientific Computing Center, a DOE Office of Science User Facility supported by the Office of Science of the U.S. Department of Energy under contract DE-AC02-05CH11231. This paper describes objective technical results and analysis. Any subjective views or opinions that might be expressed

in the paper do not necessarily represent the views of the U.S. Department of Energy or the United States Government.

Data Availability

The data that support the findings of this study are available from the corresponding author upon reasonable request.

References

Abimbola, O. P., A. R. Mittelstet, T. E. Gilmore, and J. T. Korus (2020), Influence of watershed characteristics on streambed hydraulic conductivity across multiple stream orders, *Scientific Reports*, *10*(1), 1–10, doi:10.1038/s41598-020-60658-3.

Andre, B., S. Molins, J. Johnson, and C. Steefel (2013), Alquimia, [Computer Software] https://doi.org/10.11578/dc.20210416.49, doi:10.11578/dc.20210416.49.

Aquanty, I. (2015), HydroGeoSphere User Manual, Waterloo, Ontario.

Boano, F., C. Camporeale, R. Revelli, and L. Ridolfi (2006), Sinuosity-driven hyporheic exchange in meandering rivers, *Geophysical Research Letters*, *33*(18), L18,406, doi:10.1029/2006GL027630.

Boano, F., R. Revelli, and L. Ridolfi (2007), Bedform-induced hyporheic exchange with unsteady flows, *Advances in Water Resources*, *30*(1), 148–156, doi:10.1016/j.advwatres.2006.03.004.

Boano, F., J. W. Harvey, A. Marion, A. I. Packman, R. Revelli, L. Ridolfi, and A. Wörman (2014), Hyporheic flow and transport processes: Mechanisms, models, and biogeochemical implications, *Reviews of Geophysics*, *52*(4), 603–679, doi:10.1002/2012RG000417.

Brookfield, A., C. Gnau, and B. Wilson (2017), Incorporating Surface Water Operations in an Integrated Hydrologic Model: Model Development and Application to the Lower Republican River Basin, United States, *Journal of Hydrologic Engineering*, *22*(4), 1–15, doi:10.1061/(asce)he.1943-5584.0001486.

Brunke, M. (1999), Colmation and depth filtration within streambeds: Retention of particles in hypoheic interstices, *International Review of Hydrobiology*, *84*(2), 99–117.

Calver, A. (2001), Riverbed Permeabilities: Information from Pooled Data, *Ground Water*, *39*(4), 546–553, doi:10.1111/j.1745-6584.2001.tb02343.x.

Cardenas, M. B. (2008), The effect of river bend morphology on flow and timescales of surface water-groundwater exchange across pointbars, *Journal of Hydrology*, *362*(1-2), 134–141, doi:10.1016/j.jhydrol.2008.08.018.

Cardenas, M. B. (2009a), A model for lateral hyporheic flow based on valley slope and channel sinuosity, *Water Resources Research*, *45*(1), 1–5, doi:10.1029/2008WR007442.

Cardenas, M. B. (2009b), Stream-aquifer interactions and hyporheic exchange in gaining and losing sinuous streams, *Water Resources Research*, *45*(6), W06,429, doi:10.1029/2008WR007651.

Cardenas, M. B., and J. L. Wilson (2007a), Dunes, turbulent eddies, and interfacial exchange with permeable sediments, *Water Resources Research*, *43*(8), W08,412, doi:10.1029/2006WR005787.

Cardenas, M. B., and J. L. Wilson (2007b), Exchange across a sediment-water interface with ambient groundwater discharge, *Journal of Hydrology*, *346*, 69–80, doi:10.1016/j.jhydrol.2007.08.019.

Cardenas, M. B., and V. A. Zlotnik (2003), Three-dimensional model of modern channel bend deposits, *Water Resources Research*, *39*(6), 1–13, doi:10.1029/2002WR001383.

Cardenas, M. B., J. L. Wilson, and V. A. Zlotnik (2004), Impact of heterogeneity, bed forms, and stream curvature on subchannel hyporheic exchange, *Water Resources Research*, *40*(8), W08,307, doi:10.1029/2004WR003008.

Coon, E. T., and P. Shuai (2022), Watershed Workflow: A toolset for parameterizing data-intensive, integrated hydrologic models, *Environmental Modelling Software*, *157*(July 2021), 105,502, doi:10.1016/j.envsoft.2022.105502.

Coon, E. T., D. Svyatskiy, A. Jan, E. Kikinzon, M. Berndt, A. L. Atchley, D. R. Harp, G. Manzini, E. Shelef, K. Lipnikov, R. Garimella, C. Xu, J. D. Moulton, S. Karra, S. L. Painter, E. Jafarov, and S. Molins (2019), Advanced Terrestrial Simulator (ATS)., US DOE Office of Science (SC), Biological and Environmental Research (BER), doi:10.11578/dc.20190911.1.

Coon, E. T., J. D. Moulton, E. Kikinzon, M. Berndt, G. Manzini, R. Garimella, K. Lipnikov, and S. L. Painter (2020), Coupling surface flow and subsurface flow in complex soil structures using mimetic finite differences, *Advances in Water Resources*, *144*(July), 103,701, doi:10.1016/j.advwatres.2020.103701.

Datry, T., N. Lamouroux, G. Thivin, S. Descloux, and J. M. Baudoin (2015), Estimation of Sediment Hydraulic Conductivity in River Reaches and its Potential Use to Evaluate Streambed Clogging, *River Research and Applications*, *31*(7), 880–891, doi:10.1002/rra.2784.

Dey, S., S. Saksena, D. Winter, V. Merwade, and S. McMillan (2022), Incorporating Network Scale River Bathymetry to Improve Characterization of Fluvial Processes in Flood Modeling, *Water Resources Research*, *58*(11), doi:10.1029/2020wr029521.

Dwivedi, D., C. I. Steefel, B. Arora, M. Newcomer, J. D. Moulton, B. Dafflon, B. Faybishenko, P. Fox, P. Nico, N. Spycher, R. Carroll, and K. H. Williams (2018), Geochemical Exports to River From the Intrameander Hyporheic Zone Under Transient Hydrologic Conditions: East River Mountainous Watershed, Colorado, *Water Resources Research*, *54*(10), 8456–8477, doi:10.1029/2018WR023377.

Feng, D., C. J. Gleason, X. Yang, G. H. Allen, and T. M. Pavelsky (2022), How Have Global River Widths Changed Over Time?, *Water Resources Research*, *58*(8), 1–21, doi:10.1029/2021WR031712.

Foster, L. M., K. H. Williams, and R. M. Maxwell (2020), Resolution matters when modeling climate change in headwaters of the Colorado River, *Environmental Research Letters*, *15*(10), 104,031, doi:10.1088/1748-9326/aba77f.

Genereux, D. P., S. Leahy, H. Mitasova, C. D. Kennedy, and D. R. Corbett (2008), Spatial and temporal variability of streambed hydraulic conductivity in West Bear Creek, North Carolina, USA, *Journal of Hydrology*, *358*(3-4), 332–353, doi:10.1016/j.jhydrol.2008.06.017.

Ghysels, G., S. Benoit, H. Awol, E. P. Jensen, A. Debele Tolche, C. Anibas, and M. Huysmans (2018), Characterization of meter-scale spatial variability of riverbed hydraulic conductivity in a lowland river (Aa River, Belgium), *Journal of Hydrology*, *559*, 1013–1027, doi:10.1016/j.jhydrol.2018.03.002.

Huang, P., and T. F. M. Chui (2022), Hyporheic Exchange in a Meandering Pool-Riffle Stream, *Water Resources Research*, *58*(9), doi:10.1029/2021WR031418.

Huscroft, J., T. Gleeson, J. Hartmann, and J. Börker (2018), Compiling and Mapping Global Permeability of the Unconsolidated and Consolidated Earth: GLobal HYdrogeology MaPS 2.0 (GLHYMPS 2.0), *Geophysical Research Letters*, *45*(4), 1897–1904, doi:10.1002/2017GL075860.

Jiang, P., P. Shuai, A. Sun, M. K. Mudunuru, and X. Chen (2022), Knowledge-Informed Deep Learning for Hydrological Model Calibration : An Application to Coal Creek Watershed in Colorado, (August).

Käser, D., T. Graf, F. Cochand, R. Mclaren, R. Therrien, and P. Brunner (2014), Channel Representation in Physically Based Models Coupling Groundwater and Surface Water: Pitfalls and How to Avoid Them, *Groundwater*, *52*(6), 827–836, doi:10.1111/gwat.12143.

Kolditz, O., J. O. Delfs, C. Bürger, M. Beinhorn, and C. H. Park (2008), Numerical analysis of coupled hydrosystems based on an object-oriented compartment approach, *Journal of Hydroinformatics*, *10*(3), 227–244, doi:10.2166/hydro.2008.003.

Kollet, S. J., and R. M. Maxwell (2006), Integrated surface–groundwater flow modeling: A free-surface overland flow boundary condition in a parallel groundwater flow model, *Advances in Water Resources*, *29*(7), 945–958, doi:10.1016/j.advwatres.2005.08.006.

Korus, J. T., W. P. Fraundorfer, T. E. Gilmore, and K. Karnik (2020), Transient streambed hydraulic conductivity in channel and bar environments, Loup River, Nebraska, *Hydrological Processes*, *34*(14), 3061–3077, doi:10.1002/hyp.13777.

Levy, J., M. D. Birck, S. Mutiti, K. C. Kilroy, B. Windeler, O. Idris, and L. N. Allen (2011), The impact of storm events on a riverbed system and its hydraulic conductivity at a site of induced infiltration, *Journal of Environmental Management*, *92*(8), 1960–1971, doi:10.1016/j.jenvman.2011.03.017.

Marks, K., and P. Bates (2000), Integration of high-resolution topographic data with floodplain flow models, *Hydrological Processes*, *14*(11-12), 2109–2122, doi:10.1002/1099-

1085(20000815/30)14:11/12¡2109::aid-hyp58¿3.0.co;2-1.

Maxwell, R., L. Condon, and S. Kollet (2015), A high-resolution simulation of groundwater and surface water over most of the continental us with the integrated hydrologic model parflow v3, *Geoscientific model development*, *8*(3), 923–937.

Min, L., J. Yu, C. Liu, J. Zhu, and P. Wang (2013), The spatial variability of streambed vertical hydraulic conductivity in an intermittent river, northwestern China, *Environmental Earth Sciences*, *69*(3), 873–883, doi:10.1007/s12665-012-1973-8.

Molins, S., D. Svyatsky, Z. Xu, E. T. Coon, and J. D. Moulton (2022), A Multicomponent Reactive Transport Model for Integrated Surface-Subsurface Hydrology Problems, *Water Resources Research*, *58*(8), 1–16, doi:10.1029/2022WR032074.

NOGARO, G., F. MERMILLOD-BLONDIN, F. FRANCOIS- CARCAILLET, J.-P. GAUDET, M. LAFONT, and J. GIBERT (2006), Invertebrate bioturbation can reduce the clogging of sediment: an experimental study using infiltration sediment columns, *Freshwater Biology*, *51*(8), 1458–1473, doi:10.1111/j.1365-2427.2006.01577.x.

Revelli, R., F. Boano, C. Camporeale, and L. Ridolfi (2008), Intra-meander hyporheic flow in alluvial rivers, *Water Resources Research*, *44*(12), 1–10, doi:10.1029/2008WR007081.

Salehin, M., A. I. Packman, and M. Paradis (2004), Hyporheic exchange with heterogeneous streambeds: Laboratory experiments and modeling, *Water Resources Research*, *40*(11), doi:10.1029/2003WR002567.

Sawyer, A. H., and M. B. Cardenas (2009), Hyporheic flow and residence time distributions in heterogeneous cross-bedded sediment, *Water Resources Research*, *45*(8), 1–12, doi:10.1029/2008WR007632.

Shangguan, W., T. Hengl, J. Mendes de Jesus, H. Yuan, and Y. Dai (2017), Mapping the global depth to bedrock for land surface modeling, *Journal of Advances in Modeling Earth Systems*, *9*(1), 65–88, doi:10.1002/2016MS000686.

Shrivastava, S., M. J. Stewardson, and M. Arora (2020a), Distribution of clay-sized sediments in streambeds and influence of fine sediment clogging on hyporheic exchange, *Hydrological Processes*, *34*(26), 5674–5685, doi:10.1002/hyp.13988.

Shrivastava, S., M. J. Stewardson, and M. Arora (2020b), Understanding streambeds as complex systems: review of multiple interacting environmental processes influencing streambed permeability, *Aquatic Sciences*, *82*(4), 1–18, doi:10.1007/s00027-020-00741-z.

Shuai, P., M. B. Cardenas, P. S. K. Knappett, P. C. Bennett, and B. T. Neilson (2017), Denitrification in the banks of fluctuating rivers: The effects of river stage amplitude, sediment hydraulic conductivity and dispersivity, and ambient groundwater flow, *Water Resources Research*, *53*(9), 7951–7967, doi:10.1002/2017WR020610.

Shuai, P., X. Chen, X. Song, G. E. Hammond, J. Zachara, P. Royer, H. Ren, W. A. Perkins, M. C. Richmond, and M. Huang (2019), Dam Operations and Subsurface Hydrogeology Control Dynamics of Hydrologic Exchange Flows in a Regulated River Reach, *Water Resources Research*, *55*(4), 2593–2612, doi:10.1029/2018WR024193.

Simley, J. D., and W. J. Carswell Jr (2009), The national map—hydrography, *US Geological Survey Fact Sheet*, *3054*(4).

Song, J., X. Chen, and C. Cheng (2010), Observation of bioturbation and hyporheic flux in streambeds, *Frontiers of Environmental Science Engineering in China*, *4*(3), 340–348, doi:10.1007/s11783-010-0233-y.

Storey, R. G., K. W. Howard, and D. D. Williams (2003), Factors controlling riffle-scale hyporheic exchange flows and their seasonal changes in a gaining stream: A three-dimensional groundwater flow model, *Water Resources Research*, *39*(2), 1–17, doi:10.1029/2002WR001367.

Sulis, M., C. Paniconi, and M. Camporese (2011), Impact of grid resolution on the integrated and distributed response of a coupled surface-subsurface hydrological model for the des Anglais catchment, Quebec, *Hydrological Processes*, *25*(12), 1853–1865, doi:10.1002/hyp.7941.

Thornton, P. E., R. Shrestha, M. Thornton, S.-C. Kao, Y. Wei, and B. E. Wilson (2021), Gridded daily weather data for North America with comprehensive uncertainty quantification, *Scientific Data*, *8*(1), 1–17, doi:10.1038/s41597-021-00973-0.

Tonina, D., and J. M. Buffington (2007), Hyporheic exchange in gravel bed rivers with pool-riffle morphology: Laboratory experiments and three-dimensional modeling, *Water Resources Research*, *43*(1), 1–16, doi:10.1029/2005WR004328.

Yoon, Y., M. Durand, C. J. Merry, E. A. Clark, K. M. Andreadis, and D. E. Alsdorf (2012), Estimating river bathymetry from data assimilation of synthetic SWOT measurements, *Journal of Hydrology*, *464-465*(2012), 363–375, doi:10.1016/j.jhydrol.2012.07.028.

Zarnetske, J. P., R. Haggerty, S. M. Wondzell, and M. A. Baker (2011), Dynamics of nitrate production and removal as a function of residence time in the hyporheic zone, *Journal of Geophysical Research*, *116*(G1), G01,025, doi:10.1029/2010JG001356.

Zhang, Y., and M. G. Schaap (2017), Weighted recalibration of the Rosetta pedotransfer model with improved estimates of hydraulic parameter distributions and summary statistics (Rosetta3), *Journal of Hydrology*, *547*, 39–53, doi:10.1016/j.jhydrol.2017.01.004.

Zhou, T., J. Bao, M. Huang, Z. Hou, E. Arntzen, X. Song, S. F. Harding, P. S. Titzler, H. Ren, C. J. Murray, W. A. Perkins, X. Chen, J. C. Stegen, G. E. Hammond, P. D. Thorne, and J. M. Zachara (2018), Riverbed Hydrologic Exchange Dynamics in a Large Regulated River Reach, *Water Resources Research*, pp. 2715–2730, doi:10.1002/2017WR020508.